Sensitivity of the ATLAS detector to extra dimensions in di-photon and di-lepton production processes

V. Kabachenko*, A. Miagkov† and A. Zenin

Institute for High Energy Physics, Protvino, RU 142284

Abstract

The processes of photon and lepton pair production are studied in models where gravity can propagate in large extra dimensions. The signal and backgrounds are simulated for the ATLAS detector with use of the ATLFAST program. Discovery limits are obtained and possible theoretical uncertainties for the predictions are discussed. An optimal cutoff on lepton/photon pair invariant mass which maximizes the reach in the energy scale of the extra dimension is found.

ATL-PHYS-2001-012
06/09/2001

* e-mail: kabachenko@mx.ihep.su

† e-mail: miagkov@mx.ihep.su

1 Introduction

An old idea of additional spatial dimensions is passing now through times of revival. Originally extra dimensions were thought to be compactified on a small radius of the order of the inverse Planck scale ($\sim 1/M_{Pl}$) and were thus protected from direct observations. Recently, it has been suggested that the compactification radius could be large (up to about 1 mm). This suggestion does not contradict known experimental data if one assumes that only gravity could live in the bulk with n extra dimensions, while all other fields are confined to a (3+1)-dimensional sub-space (so called 3-brane). There exist some examples in field theory of mechanisms responsible for the localization of fermions [1] and gauge bosons [2] on a brane, which indicate that the above assumption is reasonable.

Arkani-Hamed, Dimopoulos and Dvali (ADD) have developed a scenario with large extra dimensions [3] which has inspired a large number of phenomenological studies. In this scenario a new fundamental mass scale M_S of gravity in $(4+n)$D space appears. It is related to the ordinary Planck scale of gravity in 4D space and to the radius R of n additional dimensions by

$$M_{Pl}^2 \sim M_S^{n+2} R^n. \tag{1}$$

Therefore, a mass scale M_S in the TeV range is possible for $n \geq 2$ and for sufficiently large R, as permitted by present day tests of 4D Einstein gravity. This allows a Planck scale comparable with the electroweak one and gives a new perspective on the origin of a large hierarchy between the two scales.

The main consequence of the ADD scenario for particle phenomenology is the existence of an infinite tower of Kalutza-Klein (KK) excitations of the spin-2 graviton. From the 4D point of view they look like ordinary but massive gravitons with mass splitting $\sim 1/R$. Each KK graviton state interacts with the Standard Model (SM) fields very weakly, with coupling proportional to $1/M_{Pl}$, and as a result has a very long lifetime. Therefore, gravitons escape detection and one needs to sum over all gravitons with kinematically allowed masses if one is interested in calculating real graviton emissions. Large multiplicity due to the small mass splitting (in the case of real graviton production) or summation over an infinite number of gravitons (in the case of virtual graviton exchange) enhances the graviton interactions. It becomes effectively of the order of $1/M_S$ and thus, if M_S really lies in the TeV region, gravity effects can be tested in collider experiments. For $n = 2$, strong constraints are imposed by astrophysics and cosmology — $M_S > 30$ TeV [4], but for $n > 2$ a large margin exists for collider investigations.

The picture described above is the most generic consequence of the scenario and does not depend on a particular realization. Recently KK graviton manifestations in accelerator physics have been widely explored. Limits on M_S have been reported from existing experiments, as well as sensitivities at future colliders, for the ADD scenario. In the context of the ATLAS experiment at LHC, some processes with real graviton emission have been investigated in Ref. [5]. In the present work we concentrate on processes with virtual graviton exchange. In particular, we study photon and lepton

pair production in ATLAS detector.

The paper is organized as follows. In the next section we briefly review the basic steps in deriving the sum of graviton propagators which appear in the amplitudes of the processes under consideration. Also we give formulae for differential cross sections. Although they can be found elsewhere in the literature (see, e.g., Refs. [6, 7]), they are written here in a uniform manner with our notations and definition of gravity scale M_S. Section 3 presents our Monte-Carlo simulation of the processes in ATLAS. At the end of the section we discuss uncertainties in our predictions, related to the ambiguities in the summation of graviton propagators in the framework of the effective theory. In the conclusion we summarize the results of our work.

2 Virtual graviton exchange

At low energies gravity is simply described by linearized Einstein theory in $(4+n)$D. After KK reduction to 4D, assuming that the n extra dimensions are compactified on a torus, one can obtain the following spin-2 graviton interactions with the SM fields [8, 9]

$$\mathcal{L}_{eff} = -\frac{\sqrt{8\pi}}{M_{Pl}} T^{\mu\nu} \sum_k G^{(k)}_{\mu\nu}. \tag{2}$$

Here $T^{\mu\nu}$ is the usual 4D energy-momentum tensor, $G^{(k)}$ denotes individual massive KK mode of graviton and the sum is performed over all KK modes. This effective non-renormalizable lagrangian is valid, of course, for energies lower than some scale of the order of M_S. One-graviton exchange, say, in the s-channel leads to the leading order amplitude for massless fields (i.e., assuming $T^{\mu\nu}$ to be traceless)

$$\mathcal{M} = \frac{8\pi}{M_{Pl}^2} T^{\mu\nu} T_{\mu\nu} \sum_k \frac{1}{s - m^2_{(k)}}. \tag{3}$$

Due to the small mass splitting of KK modes of the graviton, the discrete sum can be replaced by an integral with an appropriate density-of-state function:

$$\sum_k \frac{1}{s - m^2_{(k)}} \to \frac{M_{Pl}^2}{M_S^{n+2}} \int_0^\infty d\, m_{(k)} \frac{m^{n-1}_{(k)}}{s - m^2_{(k)}}. \tag{4}$$

Note that the very strong suppression factor $1/M_{Pl}^2$ in eq. (3) is canceled. The integral here is divergent when $n \geq 2$ and cannot be calculated exactly without knowledge of the full theory. In this work we shall use a regularized expressions obtained by cutting off the integration at an upper limit [8]. It is natural to expect the cutoff scale to be of the order of M_S; in the present work it is put equal to M_S. Denoting $x \equiv \sqrt{s}/M_S$,

$$G(x) \equiv \frac{s^2}{M_S^{n+2}} \int_0^{M_S} d\, m_{(k)} \frac{m^{n-1}_{(k)}}{s - m^2_{(k)}}$$

$$
\begin{aligned}
&= \pi x^4 - i x^4 \log\left(\frac{1}{x^2} - 1\right), \quad (\text{for } n = 2) \\
&= \pi x^{n+2} - 2i \sum_{k=1}^{n/2-1} \frac{x^{2k+2}}{n-2k} - i x^{n+2} \log\left(\frac{1}{x^2} - 1\right), \quad (\text{for even } n > 2) \qquad (5) \\
&= \pi x^{n+2} - 2i \sum_{k=1}^{(n-1)/2} \frac{x^{2k+2}}{n-2k} + i x^{n+2} \log\left(\frac{1+x}{1-x}\right), \quad (\text{for odd } n).
\end{aligned}
$$

When $x \ll 1$ the leading contribution comes from the lowest degree of x and the expressions above give

$$G(x) \simeq -i \frac{2}{n-2} x^4 \qquad (6)$$

for all $n > 2$. The dependence on the number of extra dimensions can therefore be hidden by a redefinition of M_S. Such a prescription is mostly used in phenomenological papers[1]. However, we adopt the full expressions (5) for the summed graviton propagator for numerical calculations since there is a significant contribution to signal from subprocess energies near M_S ($x \sim 1$). For this reason each case of n extra dimensions requires a distinct consideration. We will restrict ourselves to the cases of n =2, 3, 4, and 5.

Interaction (2) leads to amplitudes growing with energy and thus violates unitarity. The energy region where unitarity becomes violated can serve as an estimate for the validity range of the effective interaction (2). In Ref. [7] unitarity restrictions from partial wave amplitudes of $\gamma\gamma \to \gamma\gamma$ scattering were considered. The full expressions (5) for the summed graviton propagator were used and the upper limit for the energy could be put equal to $0.9 M_S$ (the bound can be extracted from Figs. 3 and 4 of Ref. [7]). This cut on the energy of the subprocesses will be imposed in our numerical study of di-photon and di-lepton productions.

***pp* $\to$ $\gamma\gamma X$**

The main subprocesses here are quark-antiquark annihilation and gluon-gluon fusion

$$
\begin{aligned}
q\bar{q} &\to \gamma\gamma, \qquad (7) \\
gg &\to \gamma\gamma. \qquad (8)
\end{aligned}
$$

Both them obtain contributions from s-channel graviton exchange.

The differential cross section for the first subprocess can be written as

$$
\begin{aligned}
\frac{d\sigma}{d\cos\theta} &= \frac{\pi}{192\hat{s}} \Bigg(32\alpha^2 Q_q^4 \frac{1+\cos^2\theta}{1-\cos^2\theta} \\
&- 16\alpha Q_q^2 \,\mathrm{Im}\,[G(\hat{x})](1+\cos^2\theta) + |G(\hat{x})|^2 (1-\cos^4\theta) \Bigg), \qquad (9)
\end{aligned}
$$

[1]Generally speaking, it can happen that the underlying theory possesses extra symmetry which would lead to cancellation of this leading term (corresponding to the most powerful divergency of the integral in (4)). Type I string theory considered in Ref. [10] gives an example of such a situation. In the present work we do not assume that the cancellation takes place in the real world.

where α is the fine structure constant, Q_q is the quark charge in units of electron one, $\hat{s}$ denotes the squared total energy of the subprocess, $\hat{x} = \sqrt{\hat{s}}/M_S$ and θ is the scattering angle in center-of-mass frame. The first term is the lowest order SM contribution, while the second and third ones represent the interference between the SM and gravity and the pure graviton contribution, respectively.

As for the gluon fusion subprocess, there is no SM contribution at tree level. Nevertheless, we include the 1-loop SM amplitudes in our analysis. One should expect significant contribution to the signal from the interference term due to the large gluon luminosity at high energies at the LHC. Thus, the differential cross section in this case is as follows

$$\frac{d\sigma}{d\cos\theta} = \frac{1}{64\pi\hat{s}} \cdot \frac{1}{4} \sum_{\lambda_1,\lambda_2,\lambda_3,\lambda_4} |\mathcal{M}_{SM}^{\lambda_1\lambda_2\lambda_3\lambda_4} + \mathcal{M}_{Gr}^{\lambda_1\lambda_2\lambda_3\lambda_4}|^2. \tag{10}$$

Here the helicity amplitudes due to graviton exchange are non-zero only for two cases

$$\begin{aligned} \mathcal{M}_{Gr}^{+-+-} &= -i\frac{\pi}{\sqrt{8}} G(\hat{x})(1+\cos\theta)^2, \\ \mathcal{M}_{Gr}^{+--+} &= -i\frac{\pi}{\sqrt{8}} G(\hat{x})(1-\cos\theta)^2. \end{aligned} \tag{11}$$

The one-loop SM helicity amplitude both for massless and massive quarks in the loop can be found in Ref. [11].

***pp* $\to$ l^+l^-X**

As in the previous case we have two subprocesses

$$q\bar{q} \to l^+l^- \tag{12}$$

and

$$gg \to l^+l^-. \tag{13}$$

For the first one there are both SM and gravitational contributions to the cross section.

$$\begin{aligned} \frac{d\sigma}{d\cos\theta} &= \frac{1}{3} \cdot \frac{\pi}{128\hat{s}} \Bigg(16\pi\alpha^2 \Big((\mathcal{M}_{LL}^2 + \mathcal{M}_{RR}^2)(1+\cos\theta)^2 + (\mathcal{M}_{LR}^2 + \mathcal{M}_{RL}^2)(1-\cos\theta)^2 \Big) \\ &+ 32\alpha \,\mathrm{Im}\,[G(\hat{x})] \Big(Q_q \cos^3\theta + \frac{1}{s_W^2 c_W^2} \frac{\hat{s}}{\hat{s} - M_Z^2} (g_a^q g_a^l \frac{1-3\cos^2\theta}{2} - g_v^q g_v^l \cos^3\theta) \Big) \\ &+ |G(\hat{x})|^2 (1 - 3\cos^3\theta + 4\cos^4\theta) \Bigg) \end{aligned} \tag{14}$$

with SM chiral amplitudes

$$\mathcal{M}_{\chi_1\chi_2} = -Q_q + \frac{g_{\chi_1}^l g_{\chi_2}^q}{c_W^2 s_W^2} \cdot \frac{\hat{s}}{\hat{s} - M_Z^2}, \quad \chi_1, \chi_2 = L, R. \tag{15}$$

Here c_W and s_W are cosine and sine of the Weinberg angle, respectively, M_Z is the Z-boson mass, $g_{L(R)}^f = T_{3f} - Q_f s_W^2$ $(-Q_f s_W^2)$ with T_{3f} being third component of the fermion f isospin and $g_{a(v)}^f = (g_L^f \mp g_R^f)/2$.

For subprocess (13) the only contribution is from s-channel graviton exchange

$$\frac{d\sigma}{d\cos\theta} = \frac{\pi}{256\hat{s}}|G(\hat{x})|^2(1-\cos^4\theta). \tag{16}$$

Some remarks on $G(x)$ are worth noting. Strictly speaking, if we use the approximate expression (6), we should take into account only interference terms in cross section formulae. Otherwise the quadratic graviton contribution term, which is of order x^8, is beyond the accuracy, i.e. higher power of x, of terms neglected in eq. (5). We should then have to impose explicitly an upper cut on the center-of-mass energy to keep only $x \ll 1$, where eq. (6) is valid, or to be confident that the region where $x \sim 1$ does not give significant contribution to the signal. In the first case we lose the advantage of the LHC energy reach. These reasons are our main motivation for using the full expression eq. (5) for $G(x)$.

3 Numerical results

Simulation of the ATLAS detector was performed with the use of the ATLFAST program [12]. The main background for processes under consideration is the irreducible SM one. The cuts listed below were imposed in the analysis, both for di-photon and di-lepton production study.

- an upper limit on invariant mass $M_{\gamma\gamma/ll} \leq 0.9M_S$ was required in order not to violate unitarity and to be sure that the effective theory is valid.
- $M_{\gamma\gamma/ll} \geq 0.8$ TeV; as the main signal stems from high subprocess energy while the SM contribution decreases rapidly with energy, this cut excludes a region of poor signal and enhances the signal to background ratio.
- For the transverse momentum of the photons or the isolated leptons, we require $P_t \geq 50$ GeV.
- The photon/lepton should fall in the central region of the detector, i.e. the pseudorapidity should satisfy $|\eta| \leq 2.5$.

Let us turn to the discussions of results for particular processes.

3.1 Di-photon production in ATLAS

Here one has t- and u-channel contributions from the SM background but only an s-channel graviton contribution. Therefore, as can be seen from, e.g., eq. (9) the SM background events are mainly concentrated in the forward/backward directions, while the signal is in the central region. Fig. 1 shows the rapidity distributions which clearly illustrates this feature (Fig. 1a shows the rapidity distribution for the signal at a fixed number of extra dimensions $n = 3$ and different values of scale M_S while the distributions in Fig. 1b are for different n at fixed $M_S = 4.7$ TeV).

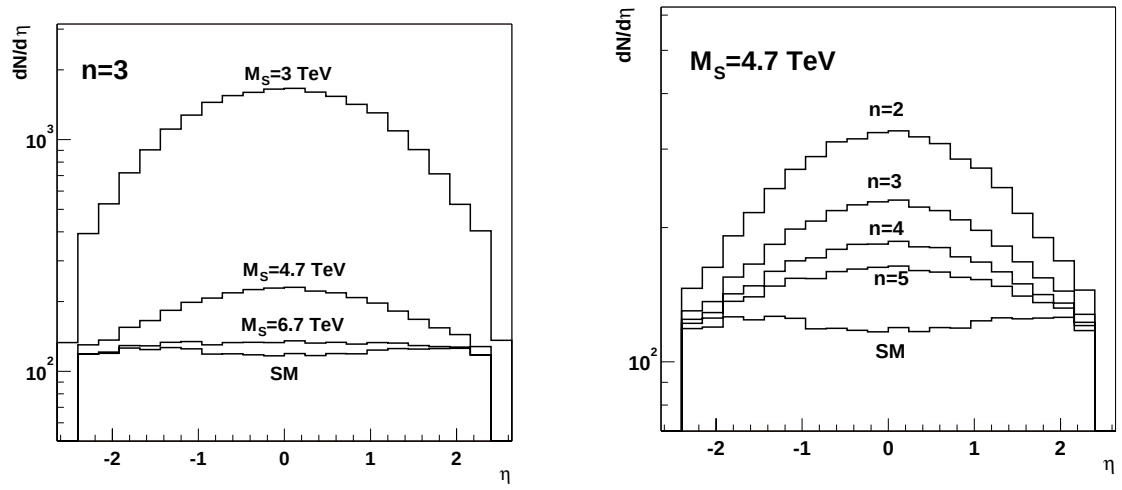

Fig. 1 Rapidity distribution of signal and background for the di-photon production: **a)** for $n = 3$ and various values of M_S; **b)** for $M_S = 4.7$ TeV and various n.

Fig. 2 presents the various event number distributions with respect to the invariant di-photon mass. In Fig. 2(a) we show the separate contributions to the signal from quark-antiquark annihilation and gluon fusion processes. Fig. 2(b) shows the total signal calculated using the full expression (5) for the summed graviton propagator as well as with only the leading term (6). One can see that the difference between the number of events in these two variants becomes significant. Fig. 2(c) and (d) present the signal at a fixed number of extra dimensions n but for different scale M_S, and at fixed M_S and different n, respectively. Note, that the truncating lines on Fig. 2(c) are at the chosen cutoff $0.9M_S$.

Both Figs. 1 and 2 shows the distributions of the real number of events in the detector at $\int \mathcal{L} dt = 10$ fb^{-1}. They were obtained with default parameters for detector resolution with the low luminosity option in ATLFAST. We have checked that switching to the high luminosity $\int \mathcal{L} dt = 100$ fb^{-1} does not influence significantly the shapes of distributions. Therefore, it is unnecessary to give the analogous pictures for high luminosity. With sufficient accuracy they could be obtained simply by multiplying by 10 all given distributions.

To estimate the sensitivity of the ATLAS detector to the parameters of the model we use the total number of registered events. The criterion $S/\sqrt{B+S} \geq 5$ gives us the maximal reach in gravity scale M_S for a fixed number n of extra dimensions at the 5σ level. Such a choice of statistical criterion gives us the possibility to use it both for large and small number of background events. As the SM background rapidly drops with invariant mass $M_{\gamma\gamma}$, imposing a lower cutoff on $M_{\gamma\gamma}$ could essentially decrease background with only moderate influence on the signal. One could expect that varying the lower cutoff allows to maximize the reach in scale. Thus, we consider the following function of two variables — lower cutoff M_{min} and M_S

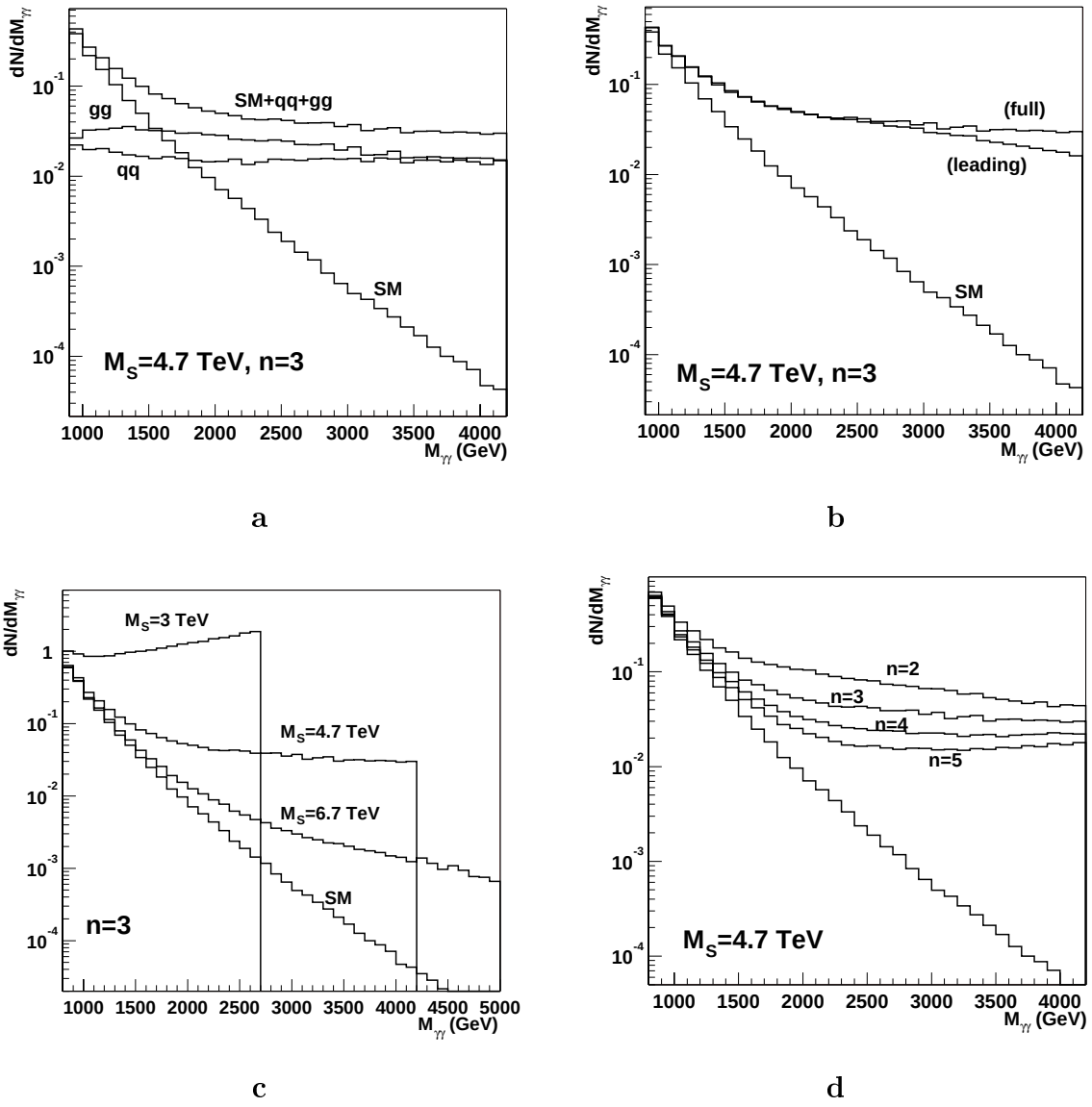

Fig. 2 Two photon invariant mass distributions: **a)** SM, separate quark and gluon contributions to the signal and total signal+background, $n = 3$, $M_S = 4.7$ TeV; **b)** total signal calculated with full expression for summed graviton propagator and only with leading term, $n = 3$, $M_S = 4,7$ TeV; **c)** total signal for $n = 3$ and various values of M_S; **d)** total signal for $M_S = 4.7$ TeV and various number n of extra dimensions.

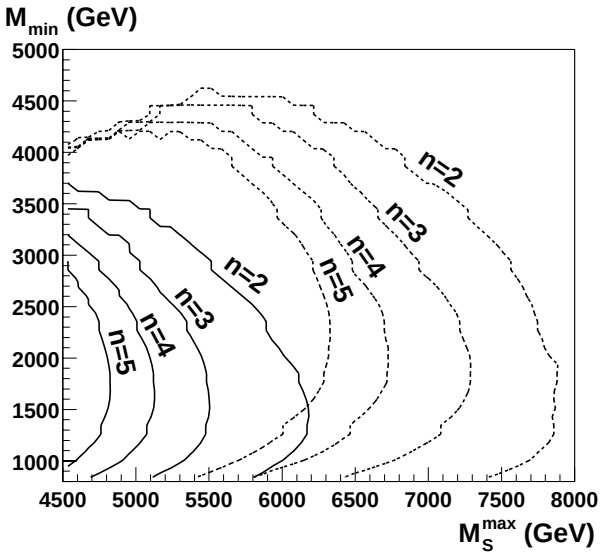

Fig. 3 Di-photon production: maximal reach at 5σ level in the scale M_S as a function of the lower cut M_{min}. Solid lines are for low luminosity $\int \mathcal{L} dt = 10$ fb^{-1}, dashed — for $\int \mathcal{L} dt = 100$ fb^{-1}. All lines are labeled by the number of extra dimensions.

$$\frac{S}{\sqrt{S+B}}(M_S, M_{min}) \equiv \int_{M_{min}}^{0.9M_S} \frac{dN_S}{dM_{\gamma\gamma}} d\,M_{\gamma\gamma} \Big/ \sqrt{\int_{M_{min}}^{0.9M_S} d\,M_{\gamma\gamma}(\frac{dN_S}{dM_{\gamma\gamma}} + \frac{dN_B}{dM_{\gamma\gamma}})}. \quad (17)$$

Fig. 3 presents the contours at 5σ level in the (M_{min}, M_S) plane for different number n of extra dimensions. We see that for each given n there exists an optimal cutoff for which the background is greatly reduced but where the statistics are still high and so the reach is maximal. The values of the maximal reach in the scale, extracted from the plot, are listed in Table 1 as well as the number of signal/backgrounds events at that scale with optimal cutoff.

3.2 Di-lepton production in ATLAS

Fig. 4 presents the results of our analysis for the di-lepton case.

In comparison with photon pair production, one can consider here an additional observable, forward-backward asymmetry. For pp collisions it is defined as follows

$$A_{FB}(M_{ll}) = \frac{(\int_0^{y_{max}} d\,y - \int_{y_{min}}^0 d\,y)(\frac{d\sigma_F}{dM_{ll}dy} - \frac{d\sigma_B}{dM_{ll}dy})}{(\int_0^{y_{max}} d\,y + \int_{y_{min}}^0 d\,y)(\frac{d\sigma_F}{dM_{ll}dy} + \frac{d\sigma_B}{dM_{ll}dy})} \quad (18)$$

where y is the rapidity of the l^+l^- system and $\sigma_{F(B)}$ is the cross section integrated over $0 < \theta < \pi/2$ ($\pi/2 < \theta < \pi$) region with θ being the scattering angle of l^- in the rest frame of the dilepton system, measured with respect to the positive direction of the z-axis. Fig. 5 shows the asymmetry as function of invariant mass M_{ll}. It is easy to understand its behavior from eqs. (14) and (16). The quadratic terms from gravity contributions are symmetric in $\cos\theta$ while the SM–gravity interference term is not. When M_{ll}, i.e. the subprocess center-of-mass energy grows,the quadratic term becomes predominant over the SM and interference ones. It cancels out in the numerator of

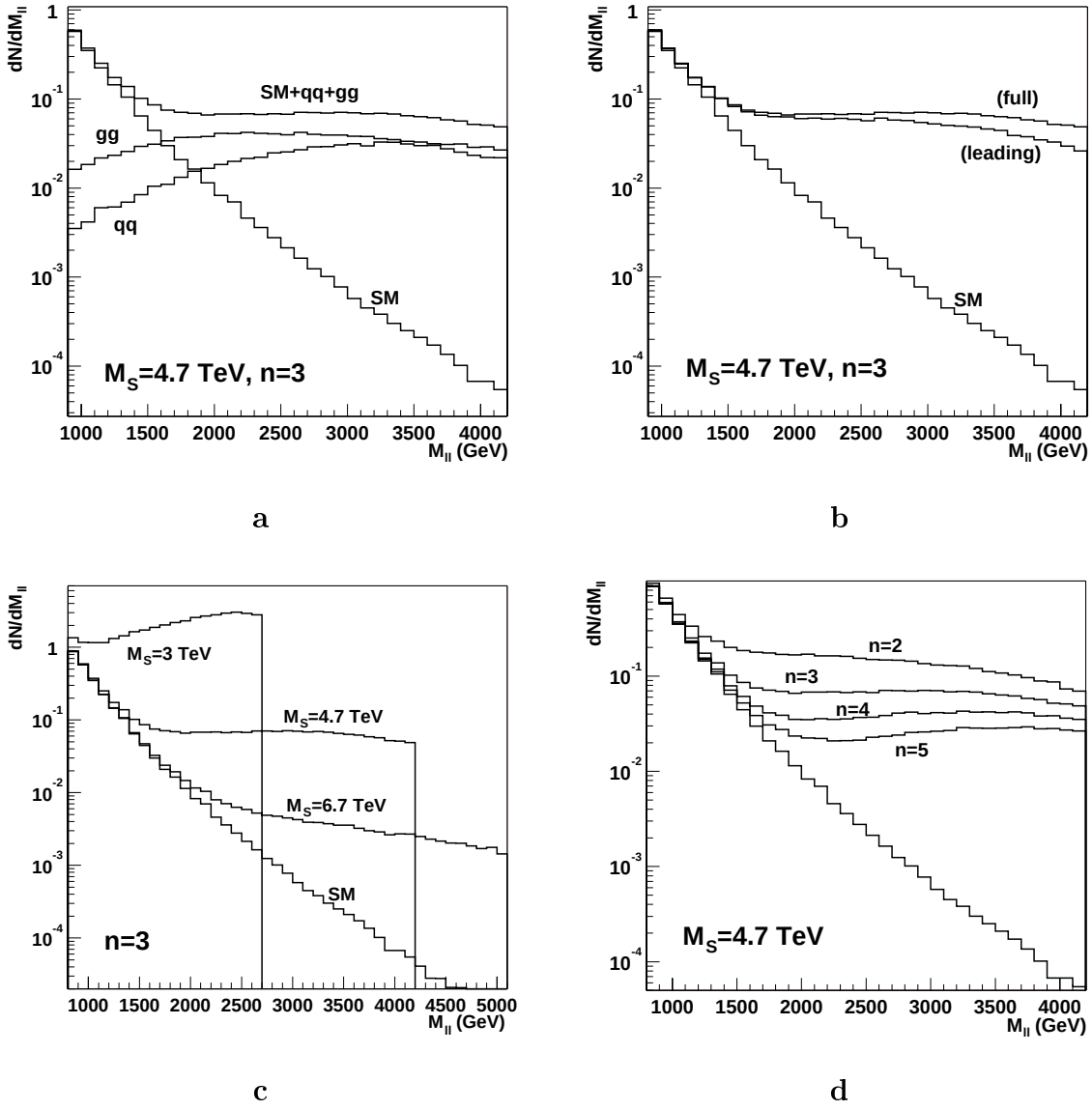

Fig. 4 The same as in Fig. 2 for the case of di-lepton production.

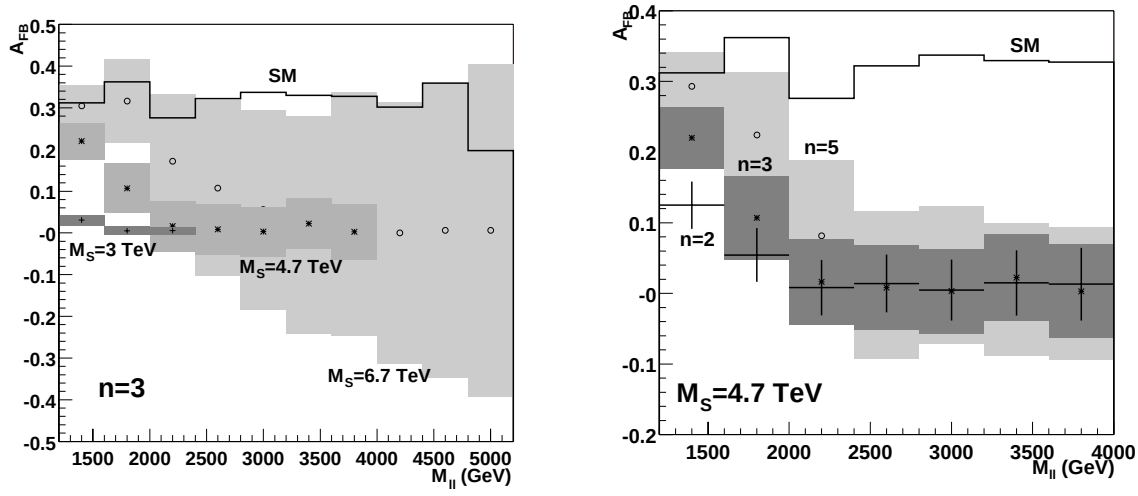

a **b**

Fig. 5 Forward-backward asymmetry as function of M_{ll}: **a)** at $n = 3$ and various values of M_S; **b)** at fixed $M_S = 4.7$ TeV and various number n of extra dimensions. Errors are presented by grey bars except for the case $n = 2$ in **(b)** where they are plotted as vertical lines. All errors correspond to high luminosity $\int \mathcal{L} dt = 100$ fb^{-1}.

of eq. (18) but dominates in the denominator. Therefore, the asymmetry approaches to zero. All errors plotted on Fig. 5 correspond to high luminosity $\int \mathcal{L} dt = 100$ fb^{-1}.

The procedure to evaluate the statistical significance of deviations from the SM predictions is the same as in the previous case. Fig. 6 shows the dependence of the achievable scale on the lower cutoff. The results for maximal reach in M_S in this channel are summarized in Table 1. We present also the maximal achievable scale which is obtained using combined statistics from both di-gamma and di-lepton channels.

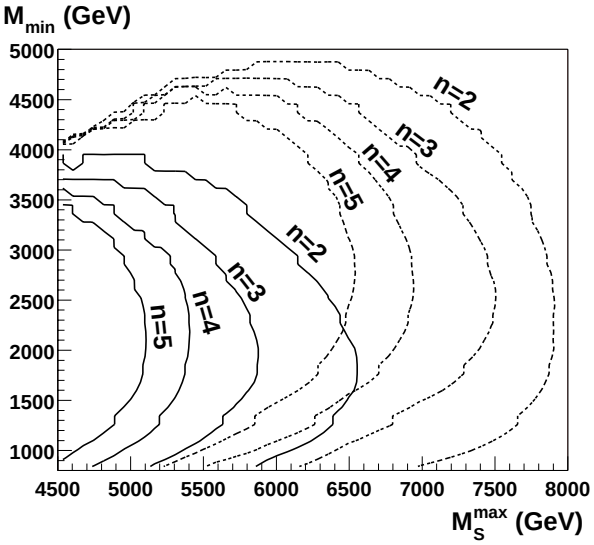

Fig. 6 Di-lepton production: maximal reach at 5σ level in the scale M_S as a function of the lower cut M_{min}. Solid lines are for low luminosity $\int \mathcal{L} dt = 10$ fb^{-1}, dashed — for $\int \mathcal{L} dt = 100$ fb^{-1}. All lines are labeled by the number of extra dimensions.

Table 1 Maximal reach in M_S at 5σ level in di-photon and di-lepton production channels as well as for combined statistics.

channel	n		2	3	4	5
	luminosiy					
$\gamma\gamma$	10 fb^{-1}	M_S^{max} (TeV)	6.3	5.6	5.1	4.9
		S/B	36/18	36/18	39/25	34/13
	100 fb^{-1}	M_S^{max} (TeV)	7.9	7.3	6.7	6.3
		S/B	50/53	62/96	55/72	51/53
l^+l^-	10 fb^{-1}	M_S^{max} (TeV)	6.6	5.9	5.4	5.1
		S/B	33/11	31/8	30/6	30/6
	100 fb^{-1}	M_S^{max} (TeV)	7.9	7.5	7.0	6.6
		S/B	49/48	38/21	36/16	29/6
$\gamma\gamma + l^+l^-$	10 fb^{-1}	M_S^{max} (TeV)	7.0	6.3	5.7	5.4
	100 fb^{-1}	M_S^{max} (TeV)	8.1	7.9	7.4	7.0

3.3 Uncertainties in predictions

The main theoretical uncertainty stems from the summation of graviton propagators. In eq. (5) only $\mathrm{Im}[iG(x)]$, i.e. the resonant contribution of the graviton, is finite, while all other terms, including the leading one at low energy, are determined by ultraviolet divergences and are sensitive to the unknown underlying theory. All physical observables thus depend on the regularization prescription for the divergent integral (4), and, strictly speaking, this dependence is unknown in the effective low energy theory . We have used the naive cutoff regularization as the simplest way to have finite quantities, although an ultraviolet cutoff dependence does not necessarily reflect the genuine dependence on the new physics scale. Nevertheless, all signal distributions given in the paper are representative of what we could expect at future experiments.

When finding the maximal achievable scale M_S as well as the optimal lower cutoff on the invariant mass, we have used the number of events integrated within the limits, which themselves depend on M_S (upper limit is $0.9M_S$). This is somewhat contradictory — in the real experiment where M_S is unknown we will deal with the total number of events. However one should expect that above $\sim M_S$, where the effective theory violates unitarity, the growth with energy of the true amplitude will be regularized by an unknown mechanism beyond the effective theory. It is natural to assume that, due to the fast decreasing effective parton luminosity with large $\hat{s}$, the contribution to the total signal of the $M_{inv} > 0.9M_S$ region would be insignificant. In any case it

seems probable that the behavior with M_S of the number of events truncated at $0.9M_S$, $\int_{M_{min}}^{0.9M_S} dM_{inv} dN/dM_{inv}$, will strongly correlate with the dependence on M_S of the total number of real events, $\int_{M_{min}}^{\sqrt{s}} dM_{inv} dN/dM_{inv}$. This consideration allows to conclude that an optimal lower cutoff, which maximizes the signal to background ratio, should really exist.

In the real experiment the values of M_S and n are unknown. To determine these values some appropriate iteration procedure should be used.

4 Conclusion

The main results of our study could be summarized as follows

- Gravity with extra dimensions could be probed with the ATLAS detector up to a scale $M_S^{max} \simeq 4.9 - 6.3(6.3 - 7.9)$ TeV for low(high) luminosity in the process of di-photon production and up to $M_S^{max} \simeq 5.1 - 6.6(6.6 - 7.9)$ TeV in the process of di-lepton production, depending on the number of extra dimensions.

- For each value of n considered, there is an optimal lower cutoff on the invariant mass, where the reach in gravity scale M_S is maximal.

- Definite correlations exist between the deviation from the SM predictions for different observables in different channels. This could allow to distinguish the scenario considered here from other SM extensions as well as from variant scenarios with different number n of extra dimensions.

- It is important "to go beyond the leading term" for the summed graviton propagator to be able to disentangle the dependence of observables on n and M_S.

The authors are grateful to A. Zaitsev for valuable discussions.

References

[1] A. V. Rubakov and M. E. Shaposhnikov, *Phys. Lett.* **B125**, 136 (1983)

[2] G. Dvali and M. Shifman, *Phys. Lett.* **B396**, 64 (1997), `hep-th/9612128`; G. Dvali, G. Gabadadze, and M. Shifman, `hep-th/0010071`

[3] N. Arkani-Hammed, S. Dimopoulos, and G. Dvali, *Phys. Lett.* **B429**, 263 (1998), `hep-ph/9803315`; *Phys. Rev.* **D59**, 086004 (1999), `hep-ph/9807344`

[4] C. Hanhart, D. R. Phillips, S. Reddy, and M. J. Savage, `nucl-th/0007178`

[5] L. Vacavant and I. Hinchliffe, "Model independent extra-dimension signature with ATLAS", ATLAS Internal Note, `hep-ex/0005033` ATL-PHYS-2000-016 (2000)

[6] K. Cheung, "Mini-review on collider signature for extra dimensions", hep-ph/0003306; J.L. Hewett, *Phys.Rev.Lett.* **82**, 4765(1999), hep-ph/9811356

[7] O. J. P. Éboli, T. Han, M. B. Magro, and P. G. Mercandante, *Phys. Rev.* **D61**, 094007 (2000), hep-ph/9908358

[8] T. Han, J. Lykken, and R.-J. Zhang, *Phys. Rev.* **D59**, 105006 (1999), hep-ph/9811350

[9] G. F. Giudice, R. Rattazzi, and J. D. Wells, *Nucl. Phys.* **B544**, 3 (1999), hep-ph/9811291

[10] E. Dudas and J. Mourad, *Nucl. Phys.* **B575**, 3 (2000), hep-ph/9911019

[11] D. A. Dicus and S. S. D. Willenbrock, *Phys. Rev.* **D37**, 1801 (1988); V. Constantini, B. De Tollis, and G. Pistoni, *Nuovo Chim.* **2A**, 733 (1971)

[12] E. Richter-Was, D. Froidevaux, and L. Poggioli, "ATLFAST 2.0: a fast simulation package for ATLAS", ATLAS Internal Note ATL-PHYS-98-131 (1998)